Scattering-based Despeckling of Multi-frequency SAR Data

A. Di Simone, G. Di Martino, A. Iodice, D. Riccio, and G. Ruello
Università di Napoli Federico II, Italy

Abstract— Speckle noise is a major factor impairing synthetic aperture radar (SAR) imagery interpretation and processing. In this paper, we propose a simple approach to deal with the despeckling of multi-frequency SAR data acquired over bare soil surfaces. The basic idea is to perform a proper normalization step in order to compensate the frequency dependence of the SAR measurements and make histograms of the multi-frequency images comparable. Once this pre-processing step is performed, conventional multi-temporal filtering can be applied. We tested this simple approach on both simulated and real-world multi-frequency datasets. Obtained results show that the proposed idea leads to increased speckle suppression capabilities with respect to both single-channel filtering and pure multi-temporal despeckling.

2023 Photonics & Electromagnetics Research Symposium (PIERS) | 979-8-3503-1284-3/23/$31.00 ©2023 IEEE | DOI: 10.1109/PIERS59004.2023.10221561

1. INTRODUCTION

Appropriate reduction of the detrimental effects of speckle noise, which typically affects coherent imaging systems, such as synthetic aperture radar (SAR), has been subject of intensive research efforts in the last decades [1]. The presence of speckle makes data interpretation difficult, but it also affects an accurate and reliable quantitative retrieval of scene physical parameters. Despeckling algorithms are often the result of a tradeoff between speckle reduction and edge/details preservation capabilities, the prior aspect depending on the application of interest. Several algorithms have been developed in the last decades to smooth speckle effects while retaining subtle details and preserving edge sharpness. Among other approaches, despeckling algorithms based on the non-local paradigm have been widely demonstrated to be one of the most effective tools in retrieving the scene reflectivity without loss of details and degradation of spatial resolution [2].

More recently, the availability of an unprecedented amount of SAR data at no cost, such as those provided by the ESA Sentinel-1 mission, has stimulated the development of multi-temporal SAR processing algorithms, including multi-temporal despeckling filters, e.g., De Grandi filter [17], UTA [18], RABASAR [19], MSAR-BM3D [3], and 2S-PPB [4]. In particular, the last two filters are the multi-temporal extension of single-channel despeckling algorithms, namely SARBM3D [5] and PPB [6], respectively.

In the more general context of multi-dimensional SAR, multi-frequency radar imagery provides more information about the surveyed scene compared with conventional single-frequency systems. As a result, many applications can effectively take advantage of multi-frequency SAR data processing, e.g., study and analysis of land cover types [9], classification [15] and snow cover analysis [14]. Different spaceborne and airborne SAR missions, such as the past SIR-C/X-SAR and AIRSAR missions and the ongoing UAVSAR operated by NASA Jet Propulsion Laboratory, have multi-frequency imaging capabilities. For instance, the AIRSAR system can simultaneously operate in fully polarimetric mode in the P- (0.45 GHz), L- (1.26 GHz), and C- (5.31 GHz) bands. The interest in multi-frequency SAR data is expected to grow further after the launch of multi-bands sensors, such as the NASA-ISRO SAR Mission (NISAR), which will gather SAR imagery of the Earth' surface at L- and S-bands, simultaneously [13].

Notwithstanding, despeckling of multi-frequency SAR imagery has been investigated in very few works, i.e., [8, 10]. In [8], a vector speckle filter which operates simultaneously in the polarization/frequency and spatial domains is developed. In [10], a non-local means method is developed based on a space-frequency information joint covariance matrix. Indeed, speckle noise affecting multi-frequency data could be faced in a naïve fashion by applying any single-channel despeckling filter to each band separately. However, it is reasonable to expect that a multi-dimensional filtering approach where all image bands are jointly filtered leads to improved speckle rejection and details preservation, thus taking advantage of the larger information amount available. As a matter of fact, multi-frequency data not only increase information content but also provide a further dimension to reduce speckle effects. Similar considerations have motivated the development of techniques for multi-temporal SAR despeckling [3].

As an alternative to single-channel filtering, multi-temporal despeckling filters might be directly applied to multi-frequency SAR series in order to somehow exploit the higher dimensionality. However, the statistical distribution of SAR imagery is greatly affected by the operating frequency, which

leads to mean bias and artifacts in most multi-temporal filter outputs, as it will be shown in our analyses. To solve such issues, here we propose a simple approach to jointly filter multi-frequency SAR data acquired over bare soil surfaces. The proposed approach consists in a pre-processing step where a frequency-calibration procedure is carried out based on the use of scattering models for compensating the dependence of SAR data upon the operating frequency. Once such a preliminary compensation step is performed, any multi-temporal filter might be applied with better mean preservation and reduced artifacts. By following the proposed approach, multi-temporal filters can more effectively applied to multi-dimensional data where the time coordinate is substituted by the frequency one.

The remainder of this paper is organized as follows: Section 2 briefly describes the scattering model adopted in the frequency-compensation step, which is described in Section 3; the effectiveness of the proposed approach is tested in Section 4 on both simulated and real-world multi-frequency SAR data. Section 5 draws the main conclusions and hints for future research activities.

2. ELECTROMAGNETIC SCATTERING MODEL

In this paper, a bare soil surface is described by means of the fractal geometry, which has been widely recognized as the best tool to describe self-similarity and self-affinity of natural land surfaces [7].

More specifically, the surveyed surface roughness is modelled as a two-dimensional (2D) fractional Brownian motion (fBm) process, i.e., a 2-D stochastic process $z(x, y)$ whose increments $z(x, y) - z(x', y')$ over a fixed horizontal distance $\tau = \sqrt{(x - x')^2 + (y - y')^2}$ are zero-mean Gaussian random variables with standard deviation $T^{1-H}\tau^H$, T being the topothesy, measured in meters, and H being the Hurst coefficient, with $0 < H < 1$, which is related to the surface fractal dimension $D = 3 - H$.

In order to describe electromagnetic scattering at microwaves from such natural surfaces, here we rely on the Small Perturbation Method (SPM), since it is described through analytical closed-form equations and shows a range of validity adequate to SAR applications and frequencies. Additionally, this method provides a very simple relation between fractals parameters and the backscattered field.

Under such assumptions, the backscattering coefficient reads as [7]

$$\sigma^0_{pq}(k) = 2\pi 8 k^{2-2H} \cos^4\theta \, |\beta_{pq}|^2 \, \frac{S_0}{(2\sin\theta)^{2+2H}} \tag{1}$$

where the subscripts p and q denote the receiving and transmitting polarization channels, respectively; k is the electromagnetic wavenumber, θ is the local incidence angle, β_{pq} accounts for the incident and reflected fields polarization and is a function of both the complex dielectric constant ε_r of the surface and the local incidence angle; S_0 characterizes the spectral behavior of the fBm surface, is measured in $[m^{(-2-2H)}]$ and is related to T and H as follows:

$$S_0 = \pi H 2^{1+2H} \frac{\Gamma(1+H)}{\Gamma(1-H)} T^{2(1-H)} \tag{2}$$

where $\Gamma(\cdot)$ is the Gamma function.

3. FREQUENCY-COMPENSATION STEP

The backscattering model in Eq. (1) states clearly and in a quantitative way the dependencies of the backscattering coefficient on the operating frequency. Apart from the factor k^{2-2H}, also β_{pq} implicitly depends upon frequency, due to the frequency variations of the complex dielectric constant of the illuminated scene. In order to explicitly assess the frequency dependence of the SAR image intensity, an image model, linking the SAR image sample intensity I to the backscattering coefficient is required. Here we adopt the following simple image model:

$$I(k_m) = \sigma^0_{pq}(k_m) A_{cell}\, n, \quad m = 1, ..., M \tag{3}$$

where k_m is the wavenumber relevant to the mth operating frequency f_m, $A_{cell} = \Delta x \Delta r$ is the resolution cell area, Δx and Δr being the azimuth and range resolution, respectively; n denotes the speckle noise, M is the number of available image bands.

Before applying pure multi-temporal filtering to the multi-frequency dataset $I(k_m)$, here we propose to normalize all available bands to a common reference wavenumber k_0, which can be defined arbitrarily.

Accordingly, the following frequency-compensation step is performed:

$$I_m(k_0) = I(k_m)\,\frac{k_0^{2-2H}}{k_m^{2-2H}} = \sigma^0_{pq}(k_0) A_{cell}\, n, \quad m = 1, ..., M \tag{4}$$

Once (4) is applied to any image band, the normalized images $I_m(k_0)$ can be regarded as the collection of M independent measurements of the reflectivity of the same scene at a common frequency f_0 and, then, application of multi-temporal filtering is meaningful. Finally, once multi-temporal filtering has been applied, the original dynamic of the intensity data can be easily restored by inverting (4).

It is worth mentioning that the proposed compensation method could, at least in principle, be followed by any multi-temporal despeckling filter, such as those discussed in Section 1. Despeckling performance evaluation might be undertaken with the support of the benchmarking framework developed in [16] for multitemporal SAR despeckling.

The normalization procedure in (4) is based on the assumption of negligible sensitivity of the dielectric constant against frequency within the range $[k_1, k_m]$. Additionally, it is worth mentioning that the proposed frequency-compensation step requires a proper estimation of the Hurst coefficient over the whole illuminated surface. To this end, the algorithm in [20] might be preliminary applied in order to retrieve the H map from the noisy images. However, for most natural surfaces and multi-temporal filters it is reasonable to assume H constant within the search window of the algorithm (whose linear size is typically of few tens of pixels), and, hence, a reference value can be used for H. Typical values of H for natural surfaces range from 0.55 to 0.95 [21].

4. RESULTS

In this Section, we test the proposed approach on both simulated and actual multi-frequency SAR images. In order to better assess the benefits of the frequency-compensation step, we compare our methodology, i.e., multi-temporal filtering applied on frequency-compensated data with pure multi-temporal filtering, i.e., without frequency compensation and with single-channel filtering. Additionally, for a fair comparison, the multi-temporal filter adopted is the extension to the multi-temporal case of the single-channel despeckling filter, i.e., they both share the same despeckling approach.

4.1. Simulated Data

Here we evaluate the benefits of the proposed normalization procedure on a simulated dataset comprising four 512×512 single-look complex images at L-, S-, C-, and X-bands. The dataset has been simulated according to the surface, scattering, and imaging models discussed in Section 2. More specifically, speckle noise is simulated as unitary-mean exponentially-distributed random process. Simulation parameters are reported in Table 1.

Table 1: Simulation parameters.

Parameter	Symbol	Value
Hurst coefficient	H	0.8
Topothesy	T	0.01 m
Dielectric constant	ε_r	4
Viewing angle	θ	30°
Frequency	f_m	[1.20, 3.20, 5.40, 9.60] GHz
Polarization	pq	HH
Azimuth resolution	Δx	1 m
Range resolution	Δr	1 m

In the frequency-compensation step, we set the reference frequency $f_0 = 1\,\text{GHz}$.

Simulation results are shown in Figure 1, where for the sake of conciseness only results relevant to the L-band are shown. Table 1 includes some synthetic quality indicators, namely mean of image (MoI), coefficient of variation (Cx), and despeckling gain (DG), which are defined, e.g., in [16]. The proposed approach [Figure 1(c)] is compared with multi-temporal filtering without frequency compensation [Figure 1(d)] and single-channel filtering [Figure 1(e)]. For single- and multi-channel

filtering, here we rely on SARBM3D and MSARBM3D filters, respectively. The benefits of the normalization procedure for speckle reduction are manifest, see Table 2.

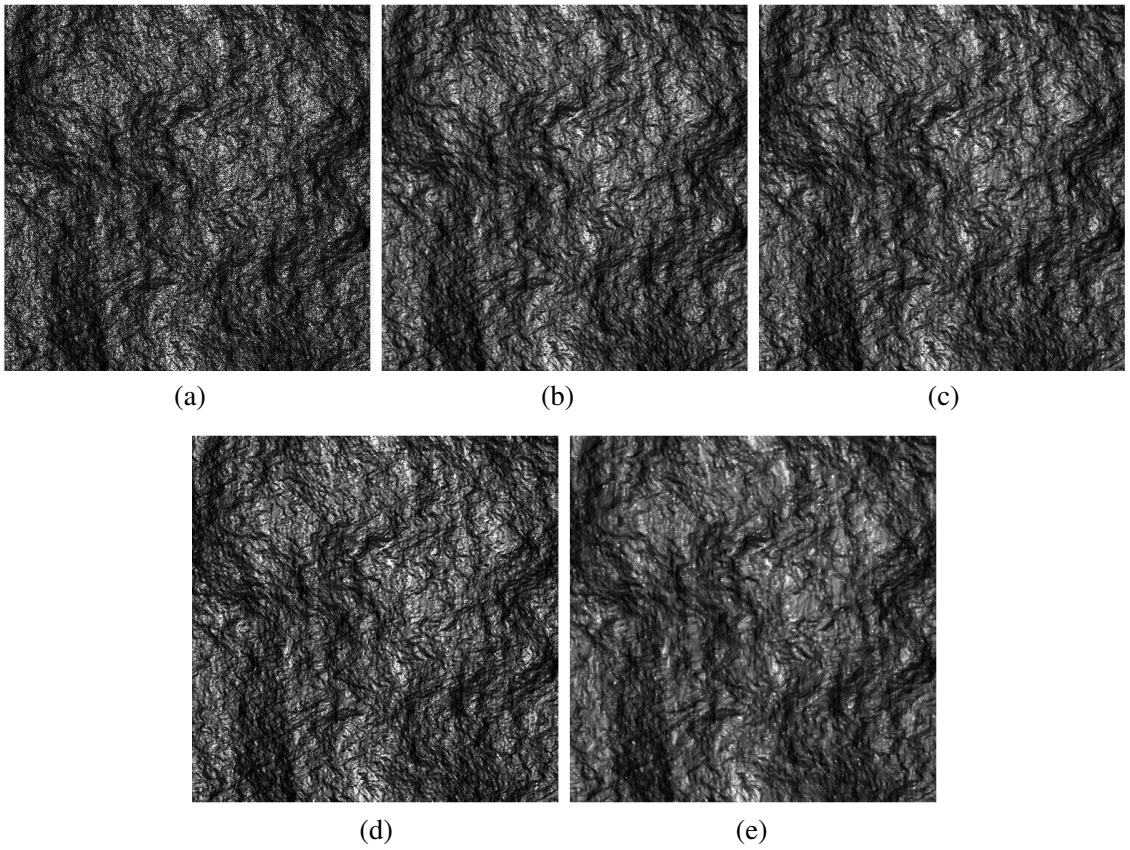

Figure 1: 512×512 L-band images: (a) noisy; (b) reference; (c) proposed approach; (d) multi-channel filtering without frequency compensation; (e) single-channel filtering.

Table 2: Despeckling performance indicators on the simulated dataset.

	MoI	C_x	DG
Reference	15.70	1.33	-
Proposed	15.44	1.35	8.71
Single-channel	15.18	1.18	6.49
Multi-Channel	15.35	1.36	8.23

4.2. Real Data

The proposed approach is here tested on a real dataset acquired from JPL AIRSAR on Flevoland on June 15, 1991. The full multi-frequency HH image is shown in Figure 2(a), while a 512×512 subset used for testing the algorithm is depicted in Figure 2(b). For this test case, we rely on 2S-PPB, MSAR-BM3D being currently implemented to work with a number of bands which is a power of two. Incidentally, this allows us to show the benefits of the frequency-compensation step on a different multi-channel filter. Accordingly, for comparison purposes, single-channel filtering is performed via PPB. Despeckling results are shown in Figures 3–5 for P-, L-, and C-band. For quantitative despeckling quality description we evaluate MoI, MoR, and ENL [the latter evaluated in the white box shown in Figure 2(b)], which are reliable no reference measures for assessing potential bias in the filtered image, see Table 3 [16]. Due to the histogram correction in the frequency-compensation step, the temporal averaging performed in 2S-PPB provides better despeckling results in terms of both mean preservation and speckle suppression, see the quality indicators in Table 3, and of bright targets maintenance especially at the lowest frequencies, see red contoured areas in Figures 3–4.

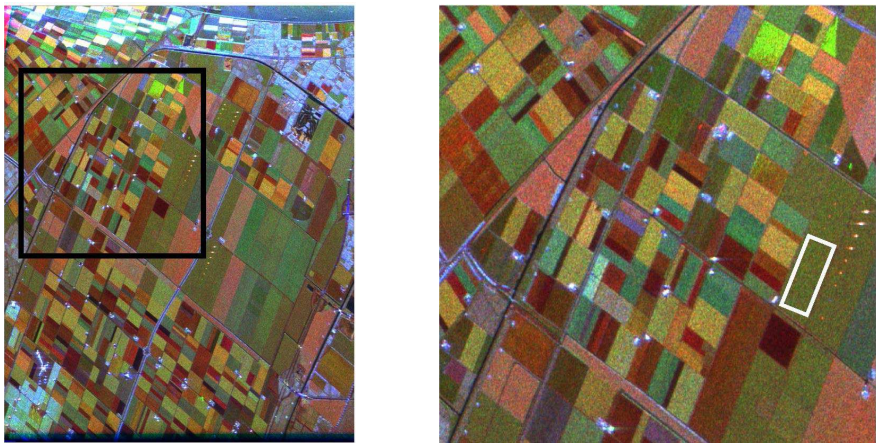

(a) (b)

Figure 2: Flevoland AIRSAR HH image (R = C-band; G = L-band; B = P-band). (a) Full scene, the black square denotes the (b) 512×512 subset. The white box indicates the area used for ENL evaluation.

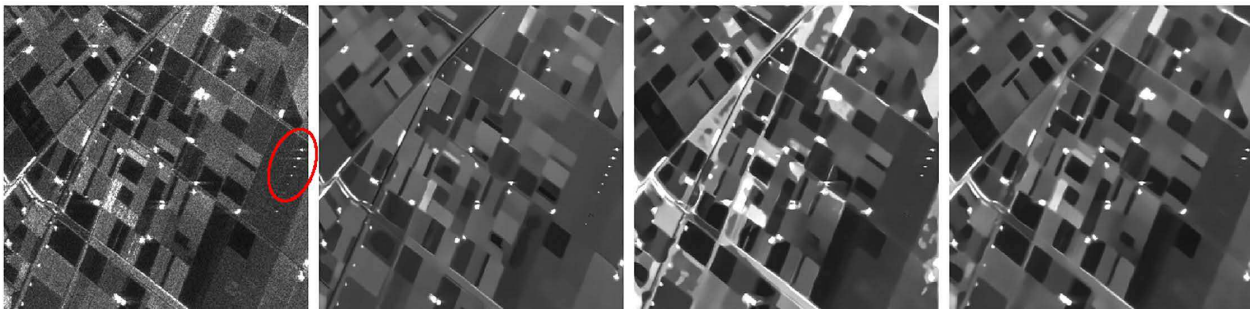

(a) (b) (c) (d)

Figure 3: Despeckling results (P-band): (a) noisy; (b) proposed approach; (c) multi-channel filtering without frequency compensation; (d) single-channel filtering.

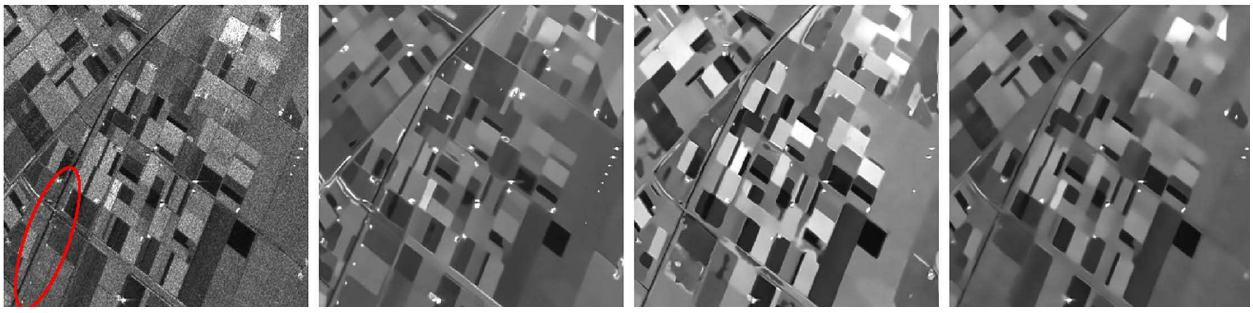

(a) (b) (c) (d)

Figure 4: Despeckling results (L-band): (a) noisy; (b) proposed approach; (c) multi-channel filtering without frequency compensation; (d) single-channel filtering.

Thanks to the normalization step, 2S-PPB recovers the mean preservation capabilities of PPB, whose results, however, presents visible widespread artifacts resembling watercolor strokes and an excessive edge smearing. In the meantime, the availability of a larger number of bands allows to the frequency-compensated multi-temporal filtering to achieve a larger ENL w.r.t. the single-channel filter.

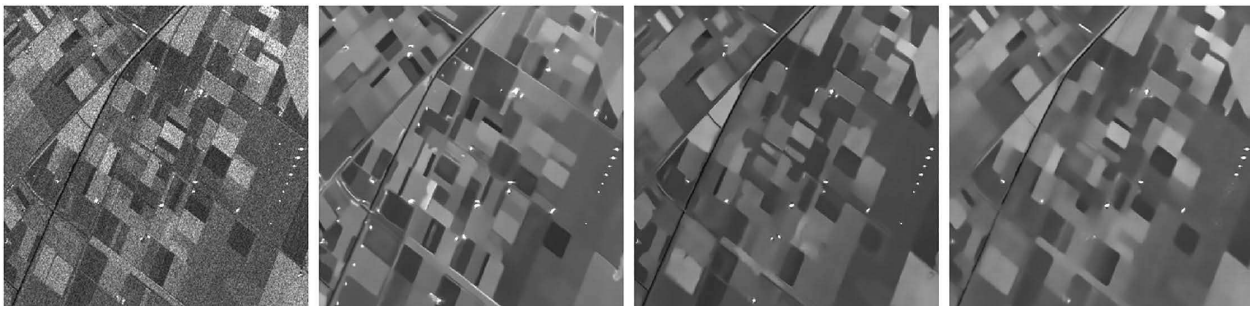

(a) (b) (c) (d)

Figure 5: Despeckling results (C-band): (a) noisy; (b) proposed approach; (c) multi-channel filtering without frequency compensation; (d) single-channel filtering.

Table 3: Despeckling performance indicators on the AIRSAR dataset.

	MoI			MoR			ENL		
	P-band	L-band	C-band	P-band	L-band	C-band	P-band	L-band	C-band
Noisy	0.0076	0.062	0.240	1	1	1	12.2	14.0	10.5
Proposed	0.0071	0.063	0.241	0.938	0.972	1.044	1049.4	911.1	830.2
Multi-channel	0.0119	0.105	0.187	0.842	0.704	1.313	716.0	297.0	154.6
Single-channel	0.0075	0.062	0.238	0.983	0.982	0.986	615.9	359.4	227.9

5. CONCLUSION

In this paper, we present a simple approach to the despeckling of multi-frequency SAR imagery acquired over bare soil surfaces. We demonstrated that, by performing a straightforward frequency-compensation procedure as a preliminary step, it is possible to improve despeckling performance of multi-temporal filters, i.e., despeckling algorithm specifically designed to deal with speckle reduction in SAR time series. Frequency calibration is based on advanced surface and scattering models which provide closed-form relationships for the modelling of the dependence of the microwave backscattered energy from surface and sensor parameters, including operating frequency. In particular, the surveyed surface is described via fractal geometry as a 2-D fBm with assigned topothesy and Hurst coefficient; surface scattering is modeled via a formulation of SPM suited to fractal surfaces. A simple image model is adopted to relate the measured SAR data intensity to the surface backscattering coefficient and then to the surface and sensors parameters. As a result, an analytical description of the dependence of SAR image intensity to the operating frequency is obtained and exploited in the frequency-compensation procedure. The compensated SAR image series can then be regarded as the series of multiple measurements of the scene reflectivity at the reference wavenumber. Accordingly, any multi-temporal despeckling filter can then be applied to the normalized dataset to obtain the filtered data.

The benefits of the calibration step have been proven on both simulated and actual multi-frequency datasets and also on different non-local means multi-temporal filters. Simulation and experimental results have shown that by properly normalizing the input image bands it is possible to improve despeckling results in terms of mean and details preservation as well as speckle suppression in homogeneous areas. With respect to multi-channel filtering, single-channel filtering does not suffer from frequency dependence of input data. However, it does not fully exploit the larger amount of information available in multi-frequency data.

It is worth noting that the exploitation of electromagnetic scattering models provides a physical basis for the extension of the proposed calibration approach to the despeckling of different multi-dimensional SAR data, e.g., multi-polarization, multi-angle, multi-sensor SAR data.

However, extension to multi-angle and/or multi-sensor data calls for the non-trivial problem of coregistering images acquired under different acquisition geometries, e.g., different viewing angles and spatial resolution. The coregistration step, unnecessary when dealing with multi-frequency sensors, such as AIRSAR, becomes crucial in such cases as it might have a non-negligible impact on the speckle statistical properties, which should be properly accounted for in the despeckling

chain. Additionally, a poor coregistration step might result in spatial resolution degradation and reduced speckle filtering capabilities.

ACKNOWLEDGMENT

This study was carried out within the Agritech National Research Center and received funding from the European Union Next-GenerationEU (PIANO NAZIONALE DI RIPRESA E RESILIENZA (PNRR) — MISSIONE 4 COMPONENTE 2, INVESTIMENTO 1.4 — D.D. 1032 17/06/2022, CN00000022). This manuscript reflects only the authors' views and opinions, neither the European Union nor the European Commission can be considered responsible for them.

REFERENCES

1. Argenti, F., A. Lapini, T. Bianchi, and L. Alparone, "A tutorial on speckle reduction in synthetic aperture radar images," *IEEE Geoscience and Remote Sensing Magazine*, Vol. 1, No. 3, 6–35, Sept. 2013.
2. Deledalle, C.-A., et al., "Exploiting patch similarity for SAR image processing: The nonlocal paradigm," *IEEE Signal Process. Mag.*, Vol. 31, No. 4, 69–78, 2014.
3. Chierchia, G., M. El Gheche, G. Scarpa, and L. Verdoliva, "Multitemporal SAR image despeckling based on block-matching and collaborative filtering," *IEEE Trans. Geosci. Remote Sens.*, Vol. 55, No. 10, 5467–5480, Oct. 2017.
4. Su, X., C.-A. Deledalle, F. Tupin, and H. Sun, "Two-step multitemporal nonlocal means for synthetic aperture radar images," *IEEE Trans. Geosci. Remote Sens.*, Vol. 52, No. 10, 6181–6196, Oct. 2014.
5. Parrilli, S., M. Poderico, C. V. Angelino, and L. Verdoliva, "A nonlocal SAR image denoising algorithm based on LLMMSE wavelet shrinkage," *IEEE Trans. Geosci. Remote Sens.*, Vol. 50, No. 2, 606–616, Feb. 2012.
6. Deledalle, C. A., L. Denis, and F. Tupin, "Iterative weighted maximum likelihood denoising with probabilistic patch-based weights," *IEEE Trans. Image Process.*, Vol. 18, No. 12, 2661–2672, Dec. 2009.
7. Franceschetti, G. and D. Riccio, *Scattering, Natural Surfaces and Fractals*, Academic, Burlington, MA, USA, 2007.
8. Lee, J.-S., M. R. Grunes, and S. A. Mango, "Speckle reduction in multipolarization, multifrequency SAR imagery," *IEEE Trans. Geosci. Remote Sens.*, Vol. 29, No. 4, 535–544, Jul. 1991.
9. Battsengel, V., D. Amarsaikhan, A. Munkh-Erdene, C. Bolorchuluun, and C. Narantsetseg, "Application of multi-frequency SAR images for knowledge acquisition," *Advances in Remote Sensing*, Vol. 2, No. 3, 242–246, 2013.
10. Ma, X., P. Wu, and H. Shen, "Multifrequency polarimetric SAR image despeckling by iterative nonlocal means based on a space-frequency information joint covariance matrix," *IEEE J. Sel. Topics Appl. Earth Observ. Remote Sens.*, Vol. 12, No. 1, 274–284, Jan. 2019.
11. Ma, X., P. Wu, Y. Wu, and H. Shen, "A review on recent developments in fully polarimetric SAR image despeckling," *IEEE J. Sel. Topics Appl. Earth Observ. Remote Sens.*, Vol. 11, No. 3, 743–758, Mar. 2018.
12. Foucher, S. and C. Lopez-Martinez, "Analysis, evaluation, and comparison of polarimetric SAR speckle filtering techniques," *IEEE Trans. Image Process.*, Vol. 23, No. 4, 1751–1764, Apr. 2014.
13. Rosen, P. A., Y. Kim, R. Kumar, T. Misra, R. Bhan, and V. R. Sagi, "Global persistent SAR sampling with the NASA-ISRO SAR (NISAR) mission," *2017 IEEE Radar Conference (RadarConf)*, 0410–0414, Seattle, WA, USA, 2017.
14. Shi, J. and J. Dozier, "On estimation of snow water equivalence using Sir-C/X-SAR," *Proc. 2nd Int. Workshop Retrieval Bio-Geo-Phys. Parameters SAR Data Land Appl.*, 503–510, Noordwijk, NL, 1998.
15. Famil, L. F., E. Pottier, and J. S. Lee, "Unsupervised classification of multifrequency and fully polarimetric SAR images based on the H/A/alpha-Wishart classifier," *IEEE Trans. Geosci. Remote Sens.*, Vol. 39, No. 11, 2332–2342, Nov. 2001.
16. Di Martino, G., A. Di Simone, A. Iodice, and D. Riccio, "Benchmarking framework for multitemporal SAR despeckling," *IEEE Trans. Geosci. Remote Sens.*, Vol. 60, 1–26, Art no. 5207826, 2022.

17. De Grandi, G. F., M. Leysen, J. S. Lee, and D. Schuler, "Radar reflectivity estimation using multiple SAR scenes of the same target: Technique and applications," *Proc. IEEE Int. Geosci. Remote Sens. Symp. Remote Sens. Sci. Vis. Sustain. Develop. (IGARSS)*, Vol. 2, 1047–1050, Aug. 1997.
18. Quegan, S., T. Le Toan, J. J. Yu, F. Ribbes, and N. Floury, "Multitemporal ERS SAR analysis applied to forest mapping," *IEEE Trans. Geosci. Remote Sens.*, Vol. 38, No. 2, 741–753, Mar. 2000.
19. Zhao, W., C.-A. Deledalle, L. Denis, H. Maitre, J.-M. Nicolas, and F. Tupin, "Ratio-based multitemporal SAR images denoising: RABASAR," *IEEE Trans. Geosci. Remote Sens.*, Vol. 57, No. 6, 3552–3565, Jun. 2019.
20. Di Martino, G., D. Riccio, and I. Zinno, "SAR imaging of fractal surfaces," *IEEE Trans. Geosci. Remote Sens.*, Vol. 50, No. 2, 630–644, Feb. 2012.
21. Franceschetti, G., A. Iodice, M. Migliaccio, and D. Riccio, "Scattering from natural rough surfaces modelled by fractional Brownian motion two-dimensional processes," *IEEE Trans. Antennas Propag.*, Vol. 47, 1405–1415, 1999.